Analysis of a Wide Radiating Slot in the Ground Plane of a Microstrip Line

Masoud Kahrizi, Tapan K. Sarkar, *Fellow, IEEE*, and Zoran A. Maricevic, *Student Member, IEEE*

***Abstract*—An analysis of a wide rectangular radiating slot excited by a microstrip line is described. Coupled integral equations are formulated to find the electric current distribution on the feed line and the electric field in the aperture. The solution is based on the method of moments and using the space domain Sommerfeld type Green's function. The information about the input impedance or reflection coefficient is extracted from the electric current distribution on the microstrip line utilizing the matrix pencil technique. The theoretical analysis is described and data are presented and compared with other theoretical and experimental results.**

I. Introduction

PRINTED circuit microstrip antennas have been extensively investigated in the last two decades. Among them slot antennas have played an important role for a variety of radar and satellite communication applications. The main advantages of radiating slots are wider bandwidth, less interaction via surface waves, better isolation and negligible radiation from feed network. Narrow slots have already been analyzed by various methods. Das and Joshi [1] have provided an expression for the complex admittance of a radiating slot in the ground plane of a microstrip line from the complex power radiated and discontinuity in the modal voltage. Their work is based upon the assumption that the electric field in the slot has a single component varying sinusoidally along the slot. A moment method solution combined with the reciprocity theorem [2] has been applied to a radiating narrow slot in the ground plane of infinitely long microstrip line. For the narrow slot, a spectral domain moment method approach is studied [3]. A related structure that used small aperture for coupling between a microstrip patch antenna and its feed line has been reported in [4]. In addition to the theoretical works, experimental results are presented for the narrow slot in the X band [5].

The wide slot antennas are of great promise. The previous assumptions are no longer valid for this case, and in practice the slot is fed by an open-ended microstrip line. In this paper, no presumption has been made for the electric surface current on the feed line. Both components of the electric fields in the slot have been considered in this analysis.

The formulation of the problem is presented in Section II and the results in the form of the three sets of linear equations are obtained. In Section III a brief discussion for the necessary Green's functions is given. The Green's functions are written in the Sommerfeld integral representation. The input impedance of the antenna or the reflection coefficient of the line is computed from the current distribution on the feed line. This method gives more accurate results about the fundamental modes and also higher order modes which exist in the vicinity of the discontinuity represented by the slot. In Section IV some numerical techniques are presented. Numerical and experimental results are given in Section V.

Manuscript received May 29, 1991; revised April 27, 1992.

The authors are with the Department of Electrical Engineering, Syracuse University, Syracuse, NY 13210.

IEEE Log Number 9204033.

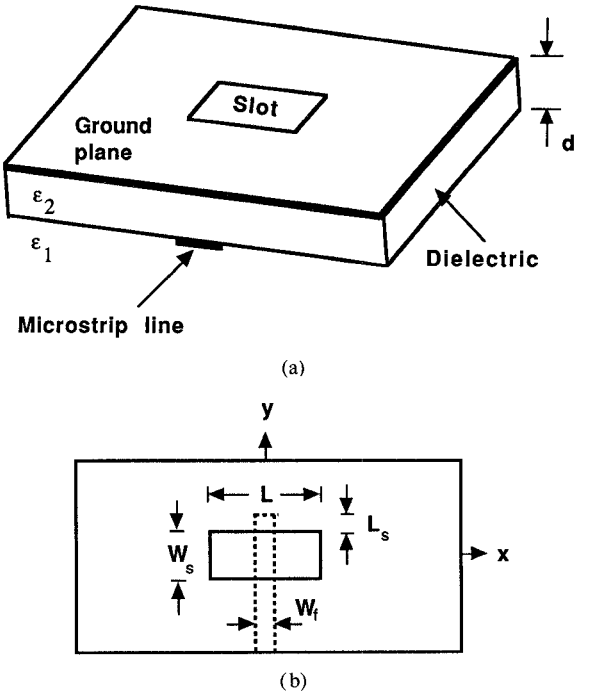

Fig. 1. Geometry of a wide slot antenna fed by an open ended microstrip line.

II. Formulation of the Analysis

Fig. 1 shows the geometry of this problem. The ground plane and dielectric substrate extend to infinity in the x and y directions. The electric surface current on the microstrip line is y-directed. The electric field across the aperture has both x and y components (Fig. 2(a)). By using the equivalence principle the aperture can be closed and then replaced by an equivalent magnetic surface current $\overline{M}_s$ below the ground plane and $-\overline{M}_s$ above the ground plane (Fig. 2(b)). The equation

$$\overline{M}_s = \hat{z} \times \overline{E}_s \tag{1}$$

relates the magnetic current $\overline{M}_s$ to the unknown electric field $\overline{E}_s$ in the slot. Therefore, we can decompose the original

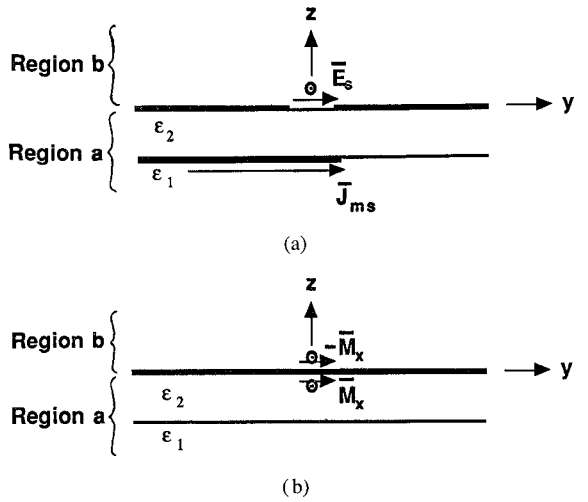

Fig. 2. Cross section of antenna with feed. (a) Original problem. (b) Equivalent problem.

problem into two isolated problems "a" and "b" (Fig. 2(b)):

1. Problem "a" is valid in the region $z < 0$ with the fields which can be generated by the magnetic current $\overline{M}_s$ and the electric current $\overline{J}_{ms}$. $\overline{J}_{ms}$ is the unknown electric surface current on the microstrip.
2. Problem "b" is valid in the region $z > 0$. The only source in this region is $-\overline{M}_s$ which radiates in the presence of the infinite perfect electric conductor plane.

The total electric and magnetic fields in the region "a" and region "b" can be written as follows:

$$\overline{E}^a_{tot} = \overline{E}^a(\overline{J}_{ms}) + \overline{E}^a(\overline{M}_s) \tag{2}$$

$$\overline{H}^a_{tot} = \overline{H}^a(\overline{J}_{ms}) + \overline{H}^a(\overline{M}_s) \tag{3}$$

$$\overline{E}^b_{tot} = \overline{E}^b(-\overline{M}_s) \tag{4}$$

$$\overline{H}^b_{tot} = \overline{H}^b(-\overline{M}_s). \tag{5}$$

Next, the preceding fields should be expressed in terms of Green's functions of a multilayer inhomogeneous region. Therefore, we can write

$$\overline{E}^a(\overline{J}_{ms}) = \iint_{ms} \overline{\overline{G}}^a_{EJ}(x,y,-d;x',y',-d) \cdot \overline{J}_{ms}(x',y')\,dx'\,dy' \tag{6}$$

$$\overline{E}^a(\overline{M}_s) = \iint_{sl} \overline{\overline{G}}^a_{EM}(x,y,-d;x',y',0) \cdot \overline{M}_s(x',y')\,dx'\,dy' \tag{7}$$

$$\overline{H}^a(\overline{J}_{ms}) = \iint_{ms} \overline{\overline{G}}^a_{HJ}(x,y,0;x',y',-d) \cdot \overline{J}_{ms}(x',y')\,dx'\,dy' \tag{8}$$

$$\overline{H}^{a,b}(\overline{M}_s) = \iint_{sl} \overline{\overline{G}}^{a,b}_{HM}(x,y,0;x',y',0) \cdot \overline{M}_s(x',y')\,dx'\,dy'. \tag{9}$$

The dyadic Green's functions can be expanded in terms of the required components such as

$$\overline{\overline{G}}^{a,b}_{HM} = \hat{x}\hat{x}G^{a,b}_{HMxx} + \hat{x}\hat{y}G^{a,b}_{HMxy} + \hat{y}\hat{x}G^{a,b}_{HMyx} + \hat{y}\hat{y}G^{a,b}_{HMyy}. \tag{10}$$

For simplicity the positional dependence of the dyadic Green's function have been omitted. However, these components depend on the position vector expressed by $G^a_{HMxy} = H_x$ at $(x,y,0)$ due to a unit y-directed magnetic current element at $(x',y',0)$ radiating in region "a".

The coupled integral equations can be obtained by enforcing the boundary conditions given below:

1. The total tangential magnetic field is continuous across the aperture.
2. The total E_y field is zero along the microstrip line surface.

Here, it should be noted that the continuity of electric field across the aperture has already been satisfied by using $\overline{M}_s$ and $-\overline{M}_s$ on different sides of the aperture. These conditions result in the following set of equations for $\overline{M}_s$ and $\overline{J}_{ms}$:

$$\overline{H}^a_{\tan}(\overline{J}_{ms}) + \overline{H}^a_{\tan}(\overline{M}_s) = \overline{H}^b_{\tan}(-\overline{M}_s), \quad \text{in the slot} \tag{11}$$

$$E^a_y(\overline{J}_{ms}) + E^a_y(\overline{M}_s) + E^{\text{inc}}_y = 0, \quad \text{on the microstrip line.} \tag{12}$$

In the above equations we have included the E^{inc}_y as the electric field due to a series voltage gap generator which affects our structure through the region "a". In the case of receiving antenna one may add the expressions for the incident field to the right hand side of (11) and (12).

We now use subsectional basis and testing functions in order to apply the method of moments. The suitable basis and testing functions for the electric and magnetic surface currents are the rooftop functions in the appropriate directions. For the electric current on the microstrip line, the line is divided into $K+1$ rectangular cells along its length all of the same dimensions $w_f \times \Delta_J$. Therefore the current can be expanded as

$$\overline{J}_{ms} = \sum_{n=1}^{K} I_n T^J_y(\overline{r} - \overline{r}^J_{yn}) \cdot \hat{y} \tag{13}$$

where

$$T^J_y(\overline{r}) = \begin{cases} 1 - \dfrac{|y|}{\Delta_J}, & |x| < w_f/2, |y| < \Delta_J \\ 0, & \text{elsewhere.} \end{cases} \tag{14}$$

The center of the nth basis function for the electric current $\overline{J}_{ms}$ is denoted by the vector $\overline{r}^J_{yn}$. By this choice, the transverse variation of the electric current on the microstrip line has been assumed to be constant, and the longitudinal distribution is to be found by this method.

In the case of the magnetic current we are facing with two dimensional currents. For this purpose, the surface of the aperture is divided into $m \times n$ rectangular cells which are chosen of equal size with dimension $\Delta_x \times \Delta_y$. $m(n)$ is the

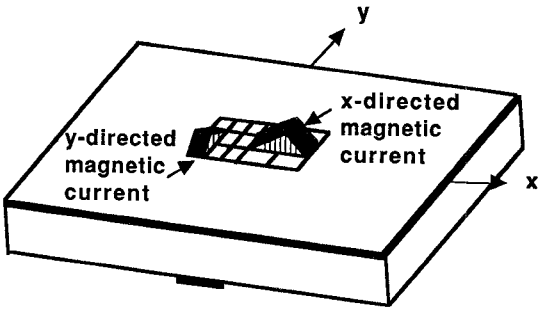

Fig. 3. Antenna with rooftop testing magnetic current.

number of divisions in $x(y)$ direction. To be more specific, referring to Fig. 3, the relations between the number of basis functions and the number of divisions are $M = (m-1)n$: The number of x- directed basis functions. $N = m(n-1)$: The number of y-directed basis functions. The magnetic currents are thus given by the expansions of the form

$$\overline{M}_s = \sum_{i=1}^{M} V_{ix} T_x^M(\overline{r} - \overline{r}_{xi}^M) + \sum_{j=1}^{N} V_{jy} T_y^M(\overline{r} - \overline{r}_{yj}^M) \quad (15)$$

where the basis functions located at the origin are defined as

$$T_x^M(\overline{r}) = \begin{cases} 1 - \dfrac{|x|}{\Delta_x}, & |x| < \Delta_x, |y| < \Delta_y/2 \\ 0, & \text{elsewhere} \end{cases} \quad (16)$$

$$T_y^M(\overline{r}) = \begin{cases} 1 - \dfrac{|y|}{\Delta_y}, & |x| < \Delta_x/2, |y| < \Delta_y \\ 0, & \text{elsewhere} \end{cases} \quad (17)$$

$\overline{r}_{xi}^M$ ($\overline{r}_{yj}^M$) is the center of $i(j)$-th $x(y)$ directed basis function.

The next step in applying the method of moment is to select the testing procedure. As testing functions, we choose the same expansion functions T_y^J, T_x^M, and T_y^M. On defining the proper Hilbert inner product in the form

$$(A, B)_s = \iint_s A^* B \, ds \quad (18)$$

where the star denotes the conjugate, the boundary condition equations lead to $K+M+N$ linear equations with $K+M+N$ unknowns which, when expressed in matrix form, are

$$\begin{bmatrix} [Z_{yy}^a] & [T_{yx}^a] & [T_{yy}^a] \\ [C_{xy}^a] & [Y_{xx}^a + Y_{xx}^b] & [Y_{xy}^a + Y_{xy}^b] \\ [D_{yy}^a] & [Y_{yx}^a + Y_{yx}^b] & [Y_{yy}^a + Y_{yy}^b] \end{bmatrix} \cdot \begin{bmatrix} [I^a] \\ [V_x] \\ [V_y] \end{bmatrix} = \begin{bmatrix} [V^i] \\ 0 \\ 0 \end{bmatrix}. \quad (19)$$

The matrix elements are defined as

$$z_{yyij}^a = (\hat{T}_y^J(\overline{r} - \overline{r}_{yi}^J), E_y^a(T_y^J(\overline{r}' - \overline{r}_{yj}^J)))_{ms} \quad (K \times K) \quad (20)$$

$$t_{yxij}^a = (\hat{T}_y^J(\overline{r} - \overline{r}_{yi}^J), E_y^a(T_x^M(\overline{r}' - \overline{r}_{xj}^M)))_{ms} \quad (K \times M) \quad (21)$$

$$c_{xyij}^a = (\hat{T}_x^M(\overline{r} - \overline{r}_{xi}^M), H_x^a(T_y^J(\overline{r}' - \overline{r}_{yj}^J)))_{sl} \quad (M \times K) \quad (22)$$

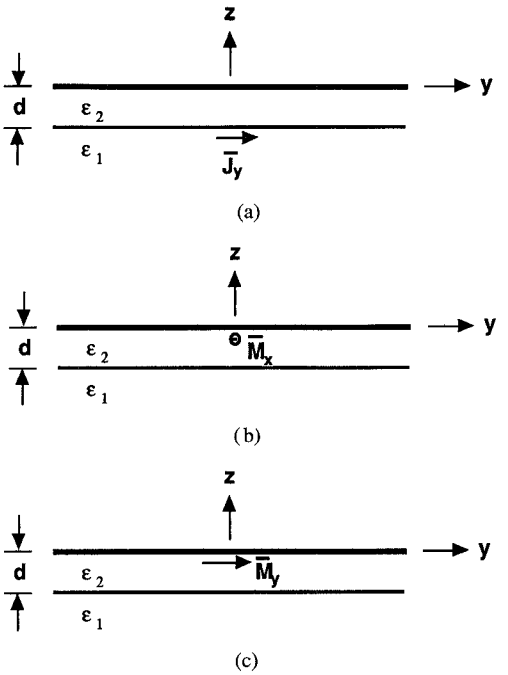

Fig. 4. Microstrip structure with three different sources. (a) y-directed HED at $z = -d$. (b) x-directed HMD at $z = 0$. (c) y-directed HMD at $z = 0$.

$$y_{xxij}^{a,b} = (\hat{T}_x^M(\overline{r} - \overline{r}_{xi}^M), H_x^{a,b}(T_x^M(\overline{r}' - \overline{r}_{xj}^M)))_{sl} \quad (M \times M) \quad (23)$$

$$d_{yyij}^a = (\hat{T}_y^M(\overline{r} - \overline{r}_{yi}^M), H_y^a(T_y^J(\overline{r}' - \overline{r}_{yj}^J)))_{sl} \quad (N \times K) \quad (24)$$

and similarly the vector elements related to excitation can be defined as

$$V_j^i = (\hat{T}_y^J(\overline{r} - \overline{r}_{yj}^J), E_y^{\text{inc}})_{ms} \quad (K \times 1) \quad (25)$$

III. Green's Functions

By definition, Green's functions are actually the potentials created by a unit source. In the structure which is considered here, we need three different cases (see Fig. 4). First a y-directed electric dipole horizontally (HED) located at $z = -d$ is studied. Second (Third) we describe $x(y)$-directed magnetic dipole horizontally (HMD) located at $z = 0$. Since the system is linear, the superposition principle can be applied to find the potentials resulting from any finite source. We now go through the details for each case.

1. y-directed HED: In this case two components of magnetic vector potential A_y, A_z are necessary to specify the field completely. The electric and magnetic fields can be derived from the magnetic vector potential by

$$\overline{E} = -j\omega\overline{A} + \frac{1}{j\omega\mu\epsilon}\nabla(\overline{\nabla} \cdot \overline{A}) \quad (26)$$

$$\overline{H} = \frac{1}{\mu}\overline{\nabla} \times \overline{A}. \quad (27)$$

Here ϵ and μ are the permittivity and permeability, respectively, of the medium whose fields are of our interest. The complete solution for the magnetic vector

potential has been given in [6], [7] and for our structure is given by

$$\left\{ \begin{matrix} A^a_{y_1}(\rho,z) \\ A^a_{y_2}(\rho,z) \end{matrix} \right\} = \frac{\mu}{4\pi}\int_c \frac{k_\rho}{D_{\mathrm{TE}}} H_0^{(2)}(k_\rho\rho) \cdot \left\{ \begin{matrix} \exp u_1(z+d) \\ \dfrac{-\sinh(u_2 z)}{\sinh(u_2 d)} \end{matrix} \right\} dk_\rho \quad \begin{matrix} \text{for } z < -d \\ \text{for } 0 > z > -d \end{matrix} \tag{28}$$

$$\left\{ \begin{matrix} A^a_{z_1}(\rho,z) \\ A^a_{z_2}(\rho,z) \end{matrix} \right\} = \frac{\mu(\epsilon_r - 1)}{4\pi}\frac{\partial}{\partial y} \cdot \int_c \frac{k_\rho}{D_{\mathrm{TE}} D_{\mathrm{TM}}} H_0^{(2)}(k_\rho\rho) \cdot \left\{ \begin{matrix} \exp u_1(z+d) \\ \dfrac{\cosh(u_2 z)}{\cosh(u_2 d)} \end{matrix} \right\} dk_\rho \quad \begin{matrix} \text{for } z < -d \\ \text{for } 0 > z > -d \end{matrix} \tag{29}$$

The notation used here will be given at the end of this section. Also

$$G^a_{EJyy} = -j\omega A^a_{y_2}(\rho,-d) + \frac{1}{j\omega\epsilon_1} \cdot \frac{\partial}{\partial y}\left(\frac{\partial}{\partial y} G^J_v(\rho,-d)\right) \tag{30}$$

where G^J_v is defined by

$$\overline{\nabla}\cdot\overline{A} = \mu\frac{\partial}{\partial y} G^J_v(\rho,z) \tag{31}$$

or

$$G^J_v(\rho,-d) = \frac{1}{4\pi}\int_c \frac{k_\rho[u_1 + u_2\tanh(u_2 d)]}{D_{\mathrm{TE}} D_{\mathrm{TM}}} \cdot H_0^{(2)}(k_\rho\rho)\, dk_\rho. \tag{32}$$

For the magnetic field components we have

$$G^a_{HJxy} = \frac{1}{\mu}\left(\frac{\partial A^a_{z_2}}{\partial y}(\rho,0) - \frac{\partial A^a_{y_2}}{\partial z}(\rho,0)\right) \tag{33}$$

$$G^a_{HJyy} = \frac{1}{\mu}\left(-\frac{\partial A^a_{z_2}}{\partial x}(\rho,0)\right) \tag{34}$$

2. x-directed HMD: Two components of electric vector potential F_x, F_z are sufficient to specify the field for this source. The electric and magnetic fields in terms of the electric vector potential are given by

$$\overline{E} = \frac{-1}{\epsilon}\overline{\nabla}\times\overline{F} \tag{35}$$

$$\overline{H} = -j\omega\overline{F} + \frac{1}{j\omega\mu\epsilon}\nabla(\overline{\nabla}\cdot\overline{F}) \tag{36}$$

After solving this problem in a similar way to HED, we obtain the complete expression for the electric vector potential as

$$\left\{ \begin{matrix} F^a_{x_1}(\rho,z) \\ F^a_{x_2}(\rho,z) \end{matrix} \right\} = \frac{\epsilon_2}{4\pi}\int_c \frac{k_\rho}{D_{\mathrm{TM}}\cosh(u_2 d)} H_0^{(2)}(k_\rho\rho) \cdot \left\{ \begin{matrix} \exp u_1(z+d) \\ \dfrac{u_1\epsilon_2}{u_2\epsilon_1}\sinh u_2(z+d) + \cosh u_2(z+d) \end{matrix} \right\} dk_\rho \quad \begin{matrix} \text{for } z < -d \\ \text{for } 0 > z > d \end{matrix} \tag{37}$$

$$\left\{ \begin{matrix} F^a_{z_1}(\rho,z) \\ F^a_{z_2}(\rho,z) \end{matrix} \right\} = \frac{\epsilon_2(\epsilon_r - 1)}{4\pi}\frac{\partial}{\partial x}\int_c \frac{k_\rho}{D_{\mathrm{TE}} D_{\mathrm{TM}}} H_0^{(2)}(k_\rho\rho) \cdot \left\{ \begin{matrix} \dfrac{\epsilon_1 \exp u_1(z+d)}{\epsilon_2\cosh(u_2 d)} \\ \dfrac{-\sinh(u_2 z)}{\sinh(u_2 d)\cosh(u_2 d)} \end{matrix} \right\} dk_\rho. \quad \begin{matrix} \text{for } z < -d \\ \text{for } 0 > z > d \end{matrix} \tag{38}$$

The expression for the required field components in this case can be written as follows:

$$G^a_{EMyx} = \frac{-1}{\epsilon_2}\left(\frac{\partial F^a_{x_2}}{\partial z}(\rho,-d) - \frac{\partial F^a_{z_2}}{\partial x}(\rho,-d)\right) \tag{39}$$

$$G^a_{HMxx} = -j\omega F^a_{x_2}(\rho,0) + \frac{-1}{j\omega\mu}\frac{\partial}{\partial x} \cdot \left(\frac{\partial}{\partial x} G^M_v(\rho,0)\right) \tag{40}$$

$$G^a_{HMyx} = \frac{1}{j\omega\mu}\frac{\partial}{\partial x}\left(\frac{\partial}{\partial x} G^M_v(\rho,0)\right) \tag{41}$$

where G^M_v is defined by

$$\overline{\nabla}\cdot\overline{F} = \epsilon_2\frac{\partial}{\partial x} G^M_v(\rho,z). \tag{42}$$

3. y-directed HMD: In a similar way we need components of electric vector potential F_y, F_z to specify the field for this source. These components are expressed by

$$\left\{ \begin{matrix} F^a_{y_1}(\rho,z) \\ F^a_{y_2}(\rho,z) \end{matrix} \right\} = \left\{ \begin{matrix} F^a_{x_1}(\rho,z) \\ F^a_{x_2}(\rho,z) \end{matrix} \right\} \quad \begin{matrix} \text{for } z < -d \\ \text{for } 0 > z > -d \end{matrix} \tag{43}$$

$$\left\{ \begin{matrix} F^a_{z_1}(\rho,z) \\ F^a_{z_2}(\rho,z) \end{matrix} \right\} = \frac{\epsilon_2(\epsilon_r - 1)}{4\pi}\frac{\partial}{\partial y}\int_c \frac{k_\rho}{D_{\mathrm{TE}} D_{\mathrm{TM}}} H_0^{(2)}(k_\rho\rho) \cdot \left\{ \begin{matrix} \dfrac{\epsilon_1 \exp u_1(z+d)}{\epsilon_2\cosh(u_2 d)} \\ \dfrac{-\sinh(u_2 z)}{\sinh(u_2 d)\cosh(u_2 d)} \end{matrix} \right\} dk_\rho. \quad \begin{matrix} \text{for } z < -d \\ \text{for } 0 > z > -d \end{matrix} \tag{44}$$

For the field components we have

$$G^a_{EMyy} = \frac{1}{\epsilon_2}\frac{\partial F^a_{z_2}}{\partial x}(\rho,-d) \tag{45}$$

$$G^a_{HMxy} = \frac{1}{j\omega\mu}\frac{\partial}{\partial x}\left(\frac{\partial}{\partial y} G^M_v(\rho,0)\right) \tag{46}$$

$$G^a_{HMyy} = -j\omega F^a_{y_2}(\rho,0) + \frac{1}{j\omega\mu}\frac{\partial}{\partial y} \cdot \left(\frac{\partial}{\partial y} G^M_v(\rho,0)\right). \tag{47}$$

Here G_v^M is defined by

$$\overline{\nabla} \cdot \overline{F} = \epsilon_2 \frac{\partial}{\partial y} G_v^M(\rho, z) \tag{48}$$

and results in the same expression as before.

Since we need to satisfy the boundary condition at $z = -d$ and $z = 0$, the z dependence can be suppressed in the final form of the Green's functions. Therefore we only have ρ dependence for these functions where ρ is the radial distance between the source point and the field point

$$\rho = \sqrt{(x - x')^2 + (y - y')^2}. \tag{49}$$

The details of the other notations are given by

$$D_{\mathrm{TE}} = u_1 + u_2 \coth(u_2 d) \tag{50}$$

$$D_{\mathrm{TM}} = \epsilon_r u_1 + u_2 \coth(u_2 d) \tag{51}$$

$$\epsilon_r = \frac{\epsilon_2}{\epsilon_1} \tag{52}$$

$$u_1 = jk_{z_1} = \sqrt{k_\rho^2 - k_1^2} \tag{53}$$

$$u_2 = jk_{z_2} = \sqrt{k_\rho^2 - k_2^2} \tag{54}$$

where $k_1 = \omega^2 \mu \epsilon_1$ and $k_2 = \omega^2 \mu \epsilon_2$. The zeros of D_{TE} and D_{TM} correspond to TE and TM surface waves, respectively. The existence of these zeros causes some problems in numerical integration.

The Green's functions related to the region "b" can be easily found from the correspondence functions in the region "a" by $d \to 0$. In the next section we will discuss the numerical techniques to carry out the result.

IV. Numerical Techniques

In order to solve (19), we need to numerically evaluate the matrix elements given in (20)–(24). These computations include a double surface integral over coordinates x, y, x', y'. Therefore, the Green's functions expressed by Sommerfeld integral have to be computed in the first step. It can be observed from (30), (33), (34), (39)–(41), (45)–(47), that the derivatives have to be taken with respect to x and y. Most of these derivatives have been transferred to the basis and testing functions by using integration by parts. However, there exist some cases in which this operation is not possible, and we have to apply the derivatives on Sommerfeld integral. Even though taking the derivative of the Sommerfeld integral could introduce some problems regarding the convergence of the original integral, this is not a problem as in our cases the source and field points are at different levels.

The Green's functions expressed in the space domain only depend on the source-to-field point distance. Therefore, they have been tabulated for a certain number of points in our structure. This number depends on the maximum distance between the source and field points. Interpolation technique has been used to compute these functions at any other point. Hence, the integral in the form

$$\int_c H_n^{(2)}(k_\rho \rho)\, f(k_\rho^2) k_\rho^{n+1} \cdot dk_\rho \tag{55}$$

has to be computed in a preliminary step. The function f and the integer n depend on the type of Green's function. The details of computing this kind of integrals are described in [6]. Here we only mention some of the important points. Numerical integration of (55) has been carried out along the real axis and by using the integral relationship

$$\int_{-\infty}^{\infty} H_n^{(2)}(k_\rho \rho)\, f(k_\rho^2) k_\rho^{n+1} \cdot dk_\rho = 2 \int_0^{\infty} J_n(k_\rho \rho)\, f(k_\rho^2) k_\rho^{n+1} \cdot dk_\rho. \tag{56}$$

In some cases the function f contains D_{TM} in the dominator. This term introduces a surface pole which must be extracted analytically prior to numerical integration. It should be noted here that we have assumed that D_{TE} has no zeros and D_{TM} has only one zero. This is true for the most of our practical purposes. In addition to surface wave pole, there exists a branch point singularity at $k_\rho = k_o$ which has been eliminated by a change of variable.

By extracting the asymptotic value of the integrand for $k_\rho \to \infty$, corresponding to the static term of the Green's function, we have obtained two benefits. First we numerically have to evaluate smoother functions which in turns increase the accuracy of the numerical integrations. Second the singularity due to zero radial distance which occurs when the source and field points are on the same cell has been removed. The asymptotic term for all cases is in the form c/ρ, where constant c depends on the type of Green's function. This subtracted term acts as another Green's function. For a rectangular cell and our rooftop testing functions, computations corresponding to this term have been done analytically. This ends our discussion for finding the unknown vector I^a, V_x, and V_y through (19).

For finding the reflection coefficient on the microstrip line, the matrix pencil technique has been used. In this technique which has been described in [8] and [9], a function has been fitted by a sum of complex exponentials. Hence the electric current $I(y)$ on the microstrip line can be given by

$$I(y) = \sum_{i=1}^{N_e} a_i e^{s_i y} \qquad y < L_s \tag{57}$$

here $y = L_s$ is the position of the open end. N_e, the number of exponentials, s_i, the complex propagation constant, and a_i the amplitude of the various exponentials have to be computed through the method. This is equivalent to numerically separating the incident wave, the reflected wave, the evanescent waves, the complex waves and/or the higher order propagating modes. The incident and reflected current wave directly define the reflection coefficient. It has been observed that in the vicinity of aperture the propagation constant for the fundamental mode is different from what we obtain for a perfect microstrip line. However, if we extract this information from the current distribution far from the discontinuity, this difference diminishes.

V. Results

In this section, the results evaluated by this technique are given and compared with other results available in the published literature.

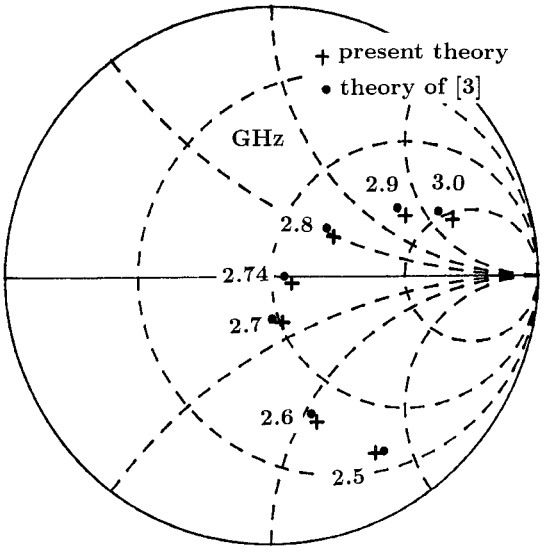

Fig. 5. Calculated input impedance of a stub-tuned narrow slot fed by a microstrip line. $\epsilon_r = 2.2, d = 0.2032$ cm. $w_f = 0.635$ cm, $w_s = 0.1016$ cm, $L = 4.0$ cm, $L_s = 0.17$ cm.

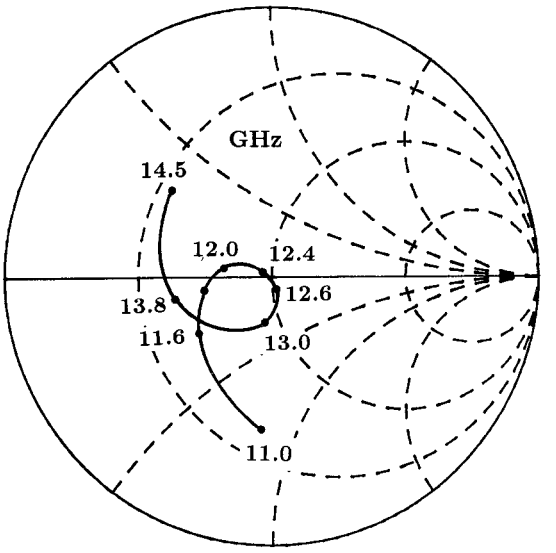

Fig. 7. Calculated input impedance of a wide slot fed by an open ended microstrip line. $\epsilon_r = 2.5, d = 0.079$ cm, $w_f = 0.025$ cm, $w_s = 0.25$ cm, $L = 0.8$ cm, $L_s = 0$ cm.

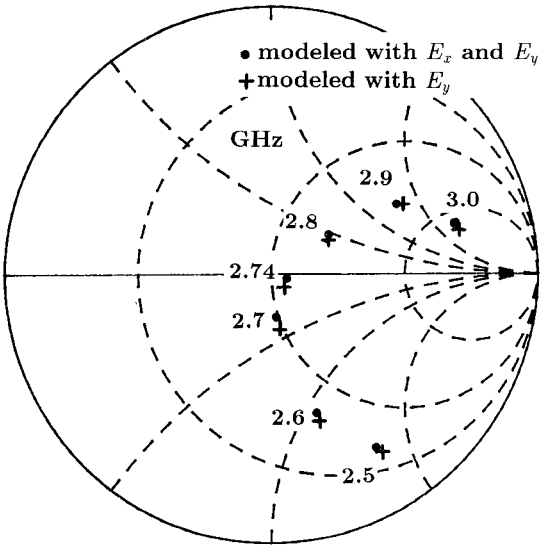

Fig. 6. Calculated input impedance of a stub-tuned narrow slot fed by a microstrip line for two kinds of modeling. $\epsilon_r = 2.2, d = 0.2032$ cm, $w_f = 0.635$ cm, $w_s = 0.1016$ cm, $L = 4.0$ cm, $L_s = 0.17$ cm.

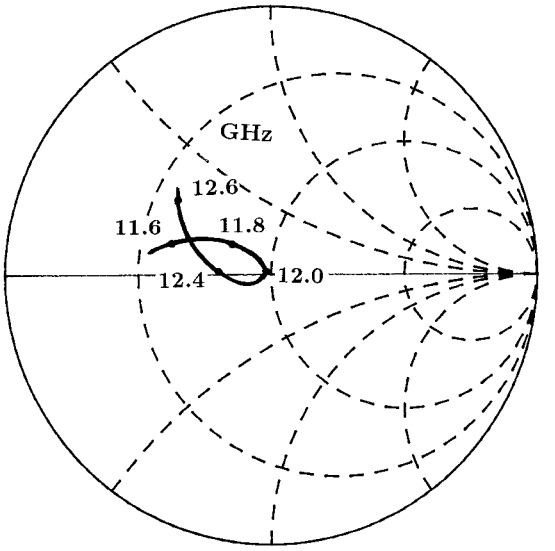

Fig. 8. Measured input impedance of a wide slot fed by an open ended microstrip line from [10]. $\epsilon_r = 2.5, d = 0.079$ cm, $w_f = 0.025$ cm, $w_s = 0.25$ cm, $L = 0.8$ cm, $L_s = 0$ cm. (a) Versus slot width. (b) Versus frequency.

Fig. 5 shows the normalized input impedance of a narrow slot of dimensions 4.0×0.1016 cm fed by a microstrip line of width $w_f = 0.635$ cm as a function of frequency calculated by this theory. The substrate parameters are $d = 0.2032$ cm, $\epsilon_r = 2.2$. The microstrip line is excited by a series voltage gap generator located at $y = -25.0$ cm. The input impedance is calculated from the reflection coefficient for the fundamental microstrip mode. For finding the reflection coefficient, current distribution on the entire structure is first solved for. Then the matrix pencil technique is used to fit the current on the line to separate the incident, reflected and other modes. From the amplitudes of the incident and reflected modes the reflection coefficient has been computed. The results for the fundamental mode are quite stable. The convergence has been insured by increasing the number of expansion functions. The reference plane in Fig. 5 is $y = 0$, the center of slot. The theoretical results of [3] are also provided in Fig. 5. The agreement between these two theories is good. Fig. 6 shows two sets of input impedance for the same slot discussed in Fig. 5. First set is for the case that we only considered the dominant component of the electric field E_y and in the second set both components of electric field have been taken into account. For the narrow slot as we expected, the results are quite close to each other. However as we increase the width of slot, the difference between these two cases increases.

The results for the input impedance of a wider slot are shown in Fig. 7. The microstrip line, of width $w_f = 0.025$ cm, on a dielectric substrate of $\epsilon_r = 2.5$, and $d = 0.079$ cm

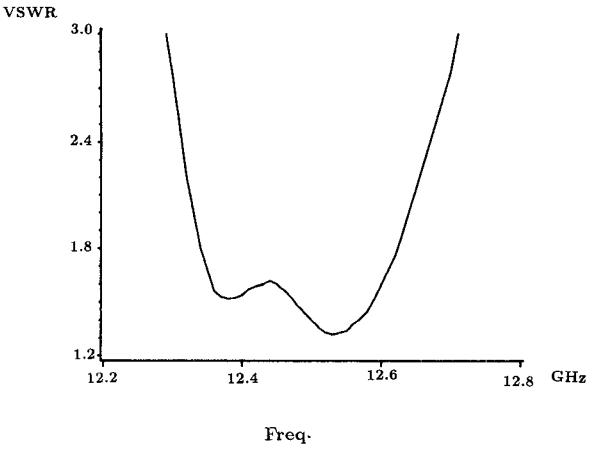

Fig. 9. VSWR of a slot antenna fed by a 50 Ω long microstrip line. $\epsilon_r = 2.5, d = 0.079$ cm, $w_f = 0.224$ cm, $w_s = 0.25$ cm, $L = 0.8$ cm.

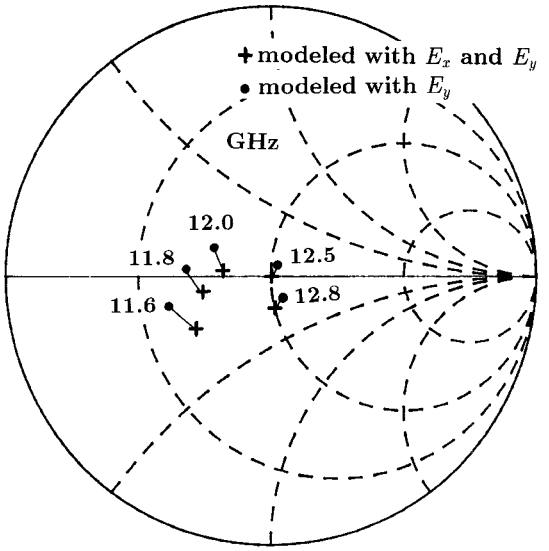

Fig. 10. Calculated input impedance of a wide slot fed by an open ended microstrip line for two kind of modeling. $\epsilon_r = 2.5, d = 0.079$ cm, $w_f = 0.025$ cm, $w_s = 0.25$ cm, $L = 0.8$ cm, $L_s = 0$ cm.

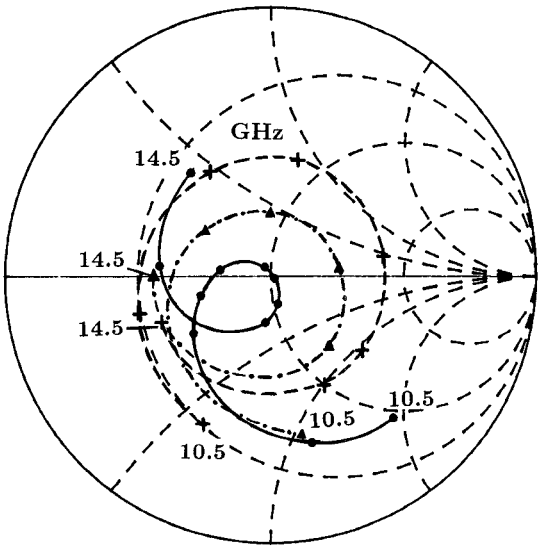

Fig. 11. Calculated input impedance as a function of stub length. $\epsilon_r = 2.5, d = 0.079$ cm, $w_f = 0.025$ cm, $w_s = 0.25$ cm, $L = 0.8$ cm.

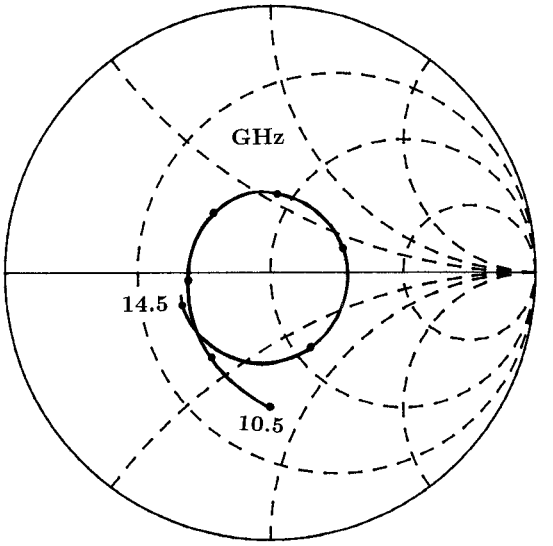

Fig. 12. Calculated input impedance for a wider slot. The reference plane is at $y = -1.9$ cm. $\epsilon_r = 2.5, d = 0.079$ cm, $w_f = 0.025$ cm, $w_s = 0.38$ cm, $L = 0.8$ cm, $L_s = 0$ cm.

has been used to excite the slot of dimensions 0.80×0.25 cm. The stub length is considered to be zero. This case has been chosen to be compared with the experimental results given in [10] as shown in Fig. 8. They show the similar behavior for the antenna. There is a shift of frequency of about 4 percent between these two plots. The reference plane for Fig. 7 is at $y = -1.98$ cm.

Fig. 9 shows the measured VSWR plot for a slot of the same dimension as Fig. 7, but in the ground plane of a 50 Ω line. The line has two open ends and each of them could be matched to a 50 Ω load. The data given in Fig. 9 allows one to determine the resonant frequency of the slot and try to match it by changing the stub length if that is possible. The region of minimum VSWR agrees well with the computed data shown in Fig. 7.

In Fig. 10 we compare the results when we ignored the x components of the electric field for the slot of Fig. 7 with the computed results when all components are considered. By comparing this result with that of Fig. 6, it becomes clear that for wider slots both components need to be considered.

The input impedance for a slot of Fig. 7 as a function of stub length L_s is illustrated in Fig. 11. Fig. 12 shows the input impedance of a slot with a different width $w_s = 0.38$ cm. By considering an extremely wide slot, we observe the necessity for considering both the components of electric field. Fig. 13 shows the difference in the calculated input impedance for a square slot.

The x and y components of electric field for the square slot of Fig. 13 are shown in Fig. 14. They are normalized magnitudes of the field components. E_x is an odd function of x as it should be because of the symmetry of the problem and satisfies the edge conditions. E_y is an even function of x. The magnitudes of E_x and E_y are quite comparable to each other.

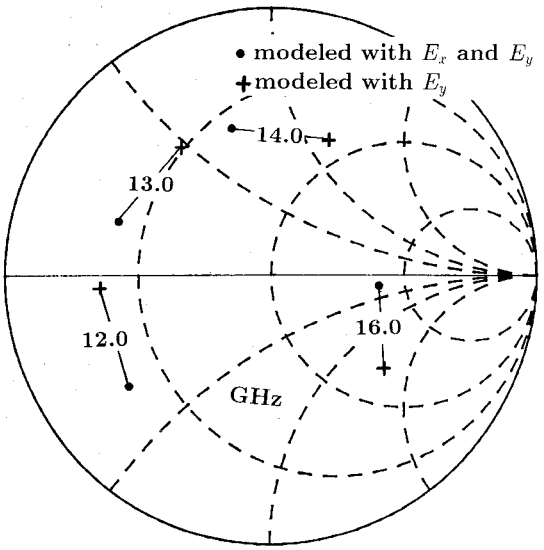

Fig. 13. Calculated input impedance of a wide slot fed by an open ended microstrip line for two kind of modeling. $\epsilon_r = 2.5, d = 0.079$ cm, $w_f = 0.025$ cm, $w_s = 0.8$ cm, $L = 0.8$ cm, $L_s = 0$ cm.

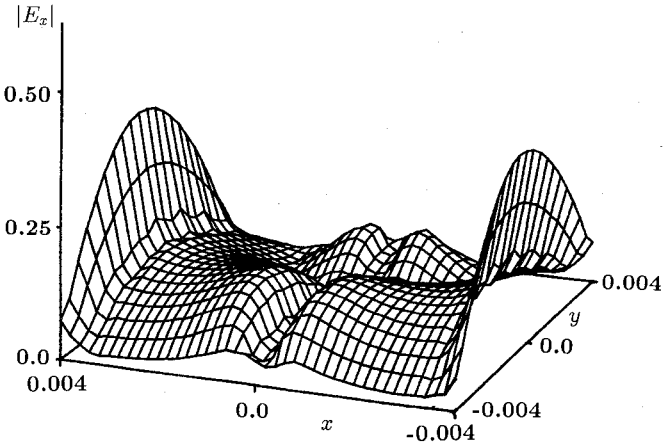

(a)

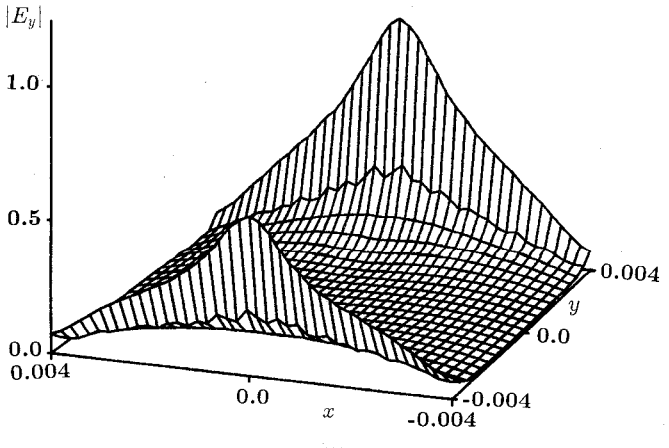

(b)

Fig. 14. Normalized x and y components of the electric field across the aperture. $\epsilon_r = 2.5, d = 0.079$ cm, $w_f = 0.025$ cm, $w_s = 0.8$ cm, $L = 0.8$ cm, $L_s = 0$ cm, Freq. = 16.0 GHz.

Therefore for a wide slot, analysis of radiation pattern should consider both components of the electric field.

VI. Conclusion

A full wave analysis for a rectangular wide slot antenna fed by a microstrip line using the method of moments and the matrix pencil method has been described. Considering both components of the electric field in the aperture leads to a reliable current distribution on the feed line. The matrix pencil method has been used to analyze this current and separate different modes on the line.

References

[1] B. N. Das and K. K. Joshi, "Impedance of a radiating slot in the ground plane of a microstrip line," *IEEE Trans. Antennas Propagat.*, vol. AP-30, pp. 922–926, Sept. 1982.

[2] D. M. Pozar, "A reciprocity method of analysis for printed slot and slot-coupled microstrip antennas," *IEEE Trans. Antennas Propagat.*, vol. AP-34, pp. 1439–1446, Dec. 1986.

[3] H. Y. Yang and N. G. Alexopoulos, "A dynamic model for microstrip-line transistion and related structures," *IEEE Trans. Microwave Theory Tech.*, vol. 36, pp. 286–293, Feb. 1988.

[4] P. L. Sullivan and D. H. Schaubert, "Analysis of an aperture coupled microstrip antenna," *IEEE Trans. Antennas Propagat.*, vol. AP-34, pp. 977–984, Aug. 1986.

[5] Y. Yoshimura, "A microstrip slot antenna," *IEEE Trans. Microwave Theory Tech.*, vol. MTT-20, pp.760–762, Nov. 1972.

[6] J. R. Mosig and T. K. Sarkar, "Comparison of quasi static and exact electromagnetic fields from a horizontal electric dipole above a lossy dielectric backed by an imperfect ground plane," *IEEE Trans. Microwave Theory and Tech.*, vol. 39, pp. 179–187, Apr. 1986.

[7] J. R. Mosig and F. E. Gardiol, "Analytical and numerical techniques in the Green's function treatment of microstrip antennas and scatterers," *Proc. Inst. Elec. Eng.*, pt. H, vol. 130, pp. 175–182, Mar. 1983.

[8] Y. Hua and T. K. Sarkar, "Matrix pencil method for estimating parameters of exponentially damped/undamped sinusoids in noise," *IEEE Trans. Acoust., Speech, Signal Processing*, vol. 38, pp. 814–824, May 1990.

[9] Z. A. Maricevic, T. K. Sarkar, Y. Hua, and A. R. Djordjevic, "Time-domain measurements with the Hewlett-Packard network analyzer HP 8510 using the matrix pencil method," *IEEE Trans. Microwave Theory Tech.*, vol. 39, pp. 538–545, Mar. 1991.

[10] M. Collier, "Microstrip antenna array for 12 GHZ TV," *Microwave J.*, vol. 20, pp. 67–71, Sept. 1977.

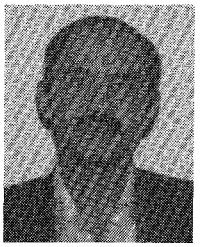

Masoud Kahrizi received the B.S. degree from Esfahan University of Technology, in 1986 and the M.S. degree from University of Tehran, Iran, in 1988, both in electrical engineering. He is currently pursuing the Ph.D. in electrical engineering from Syracuse University. His research involves the numerical problems in electromagnetics and characterization of radiating discontinuities.

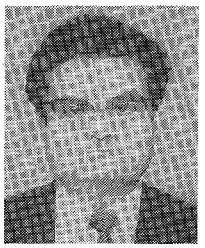

Tapan K. Sarkar (S'69–M'76–SM'81–F'91) was born in Calcutta, India, on August 2, 1948. He received the B.Tech. degree from the Indian Institute of Technology, Kharagpur, India, in 1969, the M.Sc.E. degree from the University of New Brunswick, Fredericton, Canada, in 1971, and the M.S. and Ph.D. degrees from Syracuse University, Syracuse, NY, in 1975.

From 1975 to 1976 he was with the TACO Division of General Instruments Corporation. He was with the Rochester Institute of Technology, Rochester, NY, from 1976 to 1985. He was a Research Fellow at the Gordon Mckay Laboratory, Harvard University, Cambridge, MA, from 1977 to 1978. He is now a Professor in the Department of Electrical and Computer

Engineering at Syracuse University. His current research interests deal with the numerical solution of operator equations arising in electromagnetics and signal processing with application to system design. He has authored or coauthored over 154 journal articles and conference papers and has written chapters in eight books.

Dr. Sarkar is a registered professional engineer in the state of New York. He received the Best Paper Award of the IEEE TRANSACTIONS ON ELECTROMAGNETIC COMPATIBILITY in 1979. He also received one of the "best solution" awards in May 1977 at the Rome Air Development Center (RADC) Spectral Estimation Workshop. He was an Associate Editor for feature articles of the *IEEE Antennas and Propagation Society Newsletter* and the IEEE TRANSACTIONS ON ELECTROMAGNETIC COMPATIBILITY. He was the Technical Program Chairman for the 1988 IEEE Antennas and Propagation Society International Symposium and URSI Radio Science Meeting. Dr. Sarkar is an Associate Editor for the *Journal of Electromagnetic Waves and Applications* and is on the editorial board of the *International Journal of Microwave and Millimeter-Wave Computer Aided Engineering*. He has been appointed U.S. Research Council Representative to many URSI General Assemblies. He is also Chairman of the Intercommission Working Group of International URSI on Time Domain Metrology. He is a member of Sigma Xi and the International Union of Radio Science Commissions A and B.

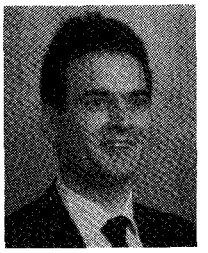

Zoran A. Maricevic (M'89–S'90) was born in Arandjelovac, Yugoslavia, on August 21, 1961. He received the Bachelor of Science in Electrical Engineering from the University of Belgrade in 1986.

Since 1988 he is the Microwave Laboratory Manager in the Department of Electrical and Computer Engineering at Syracuse University, where he is also pursuing a Ph.D. in Electrical Engineering. His research interests are in microwave measurements, numerical electromagnetics, bio-effects of electromagnetic fields and applied mathematics. He is the member of the American Geophysical Union.